EEG source space analysis of the supervised factor analytic approach for the classification of multi-directional arm movement

2017 J. Neural Eng. 14 046008

(http://iopscience.iop.org/1741-2552/14/4/046008)

IOP Publishing Journal of Neural Engineering
J. Neural Eng. **14** (2017) 046008 (14pp) https://doi.org/10.1088/1741-2552/aa6baf

EEG source space analysis of the supervised factor analytic approach for the classification of multi-directional arm movement

Vikram Shenoy Handiru[1], A P Vinod[2] and Cuntai Guan[2,3]

[1] Nanyang Institute of Technology in Health and Medicine, Interdisciplinary Graduate School, Nanyang Technological University, 50 Nanyang Avenue, Singapore 639798, Singapore
[2] School of Computer Science and Engineering, Nanyang Technological University, 50 Nanyang Avenue, Singapore 639798, Singapore
[3] Institute for Infocomm Research, Agency of Science, Technology, and Research (A∗STAR), 1 Fusionopolis Way, #20-10 Connexis North Tower, Singapore 138632, Singapore

E-mail: vikram002@e.ntu.edu.sg

Received 24 January 2017, revised 2 April 2017
Accepted for publication 6 April 2017
Published 18 May 2017

Abstract

Objective. In electroencephalography (EEG)-based brain–computer interface (BCI) systems for motor control tasks the conventional practice is to decode motor intentions by using scalp EEG. However, scalp EEG only reveals certain limited information about the complex tasks of movement with a higher degree of freedom. Therefore, our objective is to investigate the effectiveness of source-space EEG in extracting relevant features that discriminate arm movement in multiple directions. *Approach.* We have proposed a novel feature extraction algorithm based on supervised factor analysis that models the data from source-space EEG. To this end, we computed the features from the source dipoles confined to Brodmann areas of interest (BA4a, BA4p and BA6). Further, we embedded class-wise labels of multi-direction (multi-class) source-space EEG to an unsupervised factor analysis to make it into a supervised learning method. *Main Results.* Our approach provided an average decoding accuracy of 71% for the classification of hand movement in four orthogonal directions, that is significantly higher (>10%) than the classification accuracy obtained using state-of-the-art spatial pattern features in sensor space. Also, the group analysis on the spectral characteristics of source-space EEG indicates that the slow cortical potentials from a set of cortical source dipoles reveal discriminative information regarding the movement parameter, direction. *Significance.* This study presents evidence that low-frequency components in the source space play an important role in movement kinematics, and thus it may lead to new strategies for BCI-based neurorehabilitation.

Keywords: brain–computer interface, EEG source imaging, source localization, supervised factor analysis, multi class classification, multi direction hand movement

(Some figures may appear in colour only in the online journal)

1. Introduction

Brain–computer interface (BCI) systems translate the user's intention coded by brain activity measures into a control signal bypassing the normal communication pathway of muscles and peripheral nerves. These control signals can potentially be employed to substitute motor capabilities (e.g. brain-controlled prosthetics for amputees or patients with spinal cord injuries, brain-controlled wheelchair) or to help in the restoration of such functions (e.g. as a tool for stroke rehabilitation),

etc. Electroencephalography (EEG) has become an attractive modality for acquisition of brain signals for BCI due to its high temporal resolution, cost-effectiveness and portability. However, the macroscopic observation of brain signals provided by scalp EEG does not give a sufficiently accurate estimate of neural activity for many applications due to the volume conduction effect [1]. Therefore, it is challenging to interpret the neurophysiological phenomenon behind complex tasks just by observing scalp topographies generated from EEG [2–4], thus necessitating the use of cortical source-space analysis.

Electrophysiological imaging of the human brain is presented in [5] where various methods are reviewed. In the absence of functional magnetic resonance imaging (fMRI), neuroimaging can be done using inverse modeling of scalp EEG. Recent advances in high-density EEG recording and 3D source reconstruction algorithms resulted in increasingly reliable EEG source localization methods that make EEG an alternative low-cost neuroimaging tool [6]. In the past decade, the number of publications focusing on EEG source localization has surged [7–13]. There are also studies focusing on EEG source localization to classify motor imagery tasks [14, 15]. However, decoding parameters related to fine arm movement, such as type, direction and speed, has not been investigated extensively in source space. In contrast, there are sensor-space-based studies reporting the decoding of parameters such as type [16–19], speed [16, 20, 21], direction [22, 23] and force [24]. For an extensive review of non-invasive decoding of arm movement kinematics using sensor-space EEG, one can refer to [25].

As the extraction of high-dimensional cortical source features in real time is a computationally intensive task, dimension reduction techniques need to be applied when computing the features in cortical source space. Therefore, defining an anatomical region of interest (ROI) makes it easier to analyze different functional clusters by reducing the number of voxels to be processed. In the case of motor task analysis, it is a well-established fact that the primary motor cortex is involved in motor functions. There are other fMRI-based studies that report that the neuronal clusters in the primary motor cortex (also known as M1) are directionally tuned and are spatially segregated along the cortical surface [26, 27]. Task priors from the relevant ROIs have been found to result in improved classification accuracy [28].

Even though source localization and the anatomical ROI can help us appreciate the underlying neural activity of a given task, they are not sufficient *a priori* for data modeling. As there are several unknown (or rather, unobservable) cortical sources that contribute towards a given task to varying degrees, it is very difficult to model any neural observation solely based on the observable recordings irrespective of the data acquisition modality [29]. Since the scalp EEG is observable as a two-dimensional signal (electrodes $\times$ time samples) in the continuous raw data, we can refer to these observable recordings as 'manifest variables'. As the actual cortical sources are not observable directly from the scalp EEG, we refer to these cortical sources as 'latent variables'. There is a need to contemplate the behavior of underlying neurophysiological phenomena of multidirectional hand movement in terms of manifest variables and latent variables corresponding to scalp electrodes and cortical sources, respectively. Factor analysis [30] is one such algorithm that extracts the information embedded in the latent space. Santhanam *et al* has used a traditional factor analysis-based approach for neural prosthesis [29]. In that study, conducted on monkeys, they tried to explain the variability of the neural population when reach-out movement tasks are performed. The variability shown by a set of neurons is categorized into 'shared' and 'independent' variability. Shared variability is the variability that is common to different neurons for a given task, whereas independent variability corresponds to the unique neural response shown by a neuron. However, the factor analysis method presented in [29] cannot leverage the class labels as it is unsupervised. Therefore, we propose a supervised approach to learning the factor representation across classes by leveraging the spatial information of source dipoles. Our hypothesis is based on the concept of a motor homunculus which highlights that the cortical sources involved in complex movement tasks are located close together [31].

Further, the spectral characteristics of movement-related tasks are not conclusive, as there have been studies that report different frequency bands of interest ranging from delta (or slow cortical potentials <4 Hz) [32] up to high gamma (>60 Hz) [33, 34]. One should be cautious while analyzing time–frequency maps due to power-law dynamics (spectral power decreases with increasing frequencies). Some of the other related studies involving spectral characteristics of EEG cortical space features can be found in [35]. Thus, there is a need to analyze the role of different frequency bands in a multi-directional hand movement task without a lot of prior assumptions.

Our objectives in the current work are as follows. The primary goal of this work is to investigate the effectiveness of the source-space EEG in extracting useful features to discriminate arm movement directions. Further, instead of relying on traditional feature extraction methods, we propose a novel supervised factor analytic approach which, we believe, helps in better data interpretation. Also, we put forward our approach to help visualize the cortical source features that are more relevant to a given movement direction stimulus. To the best of our knowledge, there are very few studies that use cortical source-space information to extract discriminative features to decode the direction of arm movement from EEG. Therefore, we bring in our main contribution towards discriminating features by modifying classical unsupervised factor analysis to a supervised approach by embedding class-wise label information.

The remainder of this paper is organized as follows: section 2 presents the participants, data acquisition, experimental setup and preprocessing; section 3 explains our proposed methodology highlighting the EEG source imaging and our novel feature extraction technique. Section 4 presents the results, followed by a discussion in section 5. Section 6 concludes the paper.

2. Materials

2.1. Participants

Seven healthy right-handed participants (all male, age range 25–36 years, mean 31 ± 4.4 (SD)) took part in this experiment. All participants gave written informed consent before participation. The experimental protocol was approved by

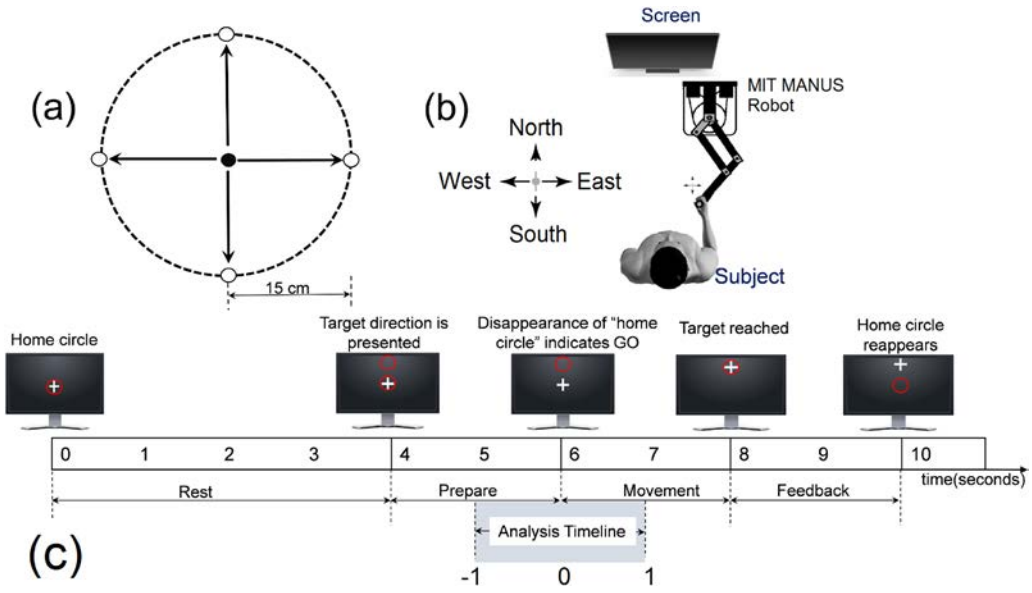

Figure 1. Experimental setup and task timeline. (a) Direction cues for 2D center-out movements are shown with the dark filled circle at the center referred to as the initial 'Home', and the target circle (blank circle on the circumference) indicating the final position. (b) Experimental setup including the reaching apparatus—a MIT MANUS robot. (c) Task timeline for the direction cue 'NORTH'. The EEG recorded during the 'Analysis Timeline' has been used for further processing.

the local Institutional Review Board of the Neural Signal Processing Laboratory at the Institute for Infocomm Research (I2R), Singapore.

2.2. Data acquisition

EEG was continuously recorded from 118 electrodes out of a 128-channel Quickcap placed on each subject's head, according to the extended International 10–20 system. A Neuroscan SynAmps2 amplifier was used to record the EEG data during the experiment conducted at the Brain–Computer Interface Laboratory at the Institute for Infocomm Research, Singapore. Continuous EEG data were sampled at 250 Hz, followed by band-pass filtering between 0.5 Hz and 100 Hz. Subsequent data analysis was performed offline using custom-written MATLAB® code.

2.3. Experimental setup

Our experimental setup involved center-out right-hand movement in four directions (north, south, east and west) using the MIT-MANUS robotic arm [36] as indicated in figure 1. 'North' indicates the movement of the subject's hand outward and away from the body, 'south' indicates the subject's hand movement inward and toward the body. Similarly, 'west' and 'east' correspond to movement towards the left and right, respectively. In this experiment, subjects were seated in front of a monitor, and they were instructed to hold the MIT-MANUS robot arm with their right hand while their left hand rested on the table. The display monitor was placed at a comfortable viewing distance of about 60 cm in front of the subject. The cursor was shown in the form of a plus sign. The target was a circle of 1 cm radius displayed on the screen, initially positioned at the center. Every trial began with a rest period of 4 s, and then visual cues were shown on the screen as a cursor and a target circle. Based on a randomized stimulus, the target circle shifted from the center of the screen to another position on the screen corresponding to the direction cue, allowing the subject to plan his hand movement in the direction instructed. The target circle remained at its new position for 2 s, after which the home circle disappeared, thus signaling the subject to move his hand. The center-to-target distance was about 15 cm. Subjects performed a task of center-out movement by moving the robot arm to match a cursor with a target circle shown on the screen during one of the four conditions. The robot recorded different kinematic parameters such as position, velocity and force applied. Subjects were instructed to finish their movement from center-to-target (distance 15 cm) within 0.5 s to avoid confusion regarding the duration of the reach. Moreover, the movement accuracy was not very critical as the task required only coarse movement to the target direction. None of the trials were rejected based on the movement trajectory information. The position of the target circle was continuously presented throughout the experiment. Electro-oculography (EOG) was also recorded to monitor eye movement. A total of 40 trials for each direction were recorded for each subject, thus resulting in 160 trials in four directions.

2.4. Preprocessing

EEG results recorded from all 118 channels were used for the analysis. Since our objective is to use the cortical time-series information for better feature extraction, we used a dense EEG headset as suggested in [12]. Trial segmentation is based on randomized trial codes corresponding to the hand movement in 'east,' 'west,' 'north' and 'south' directions, analogous to 'right', 'left', 'forward' and 'backward' directions, respectively. Continuous EEG was segmented

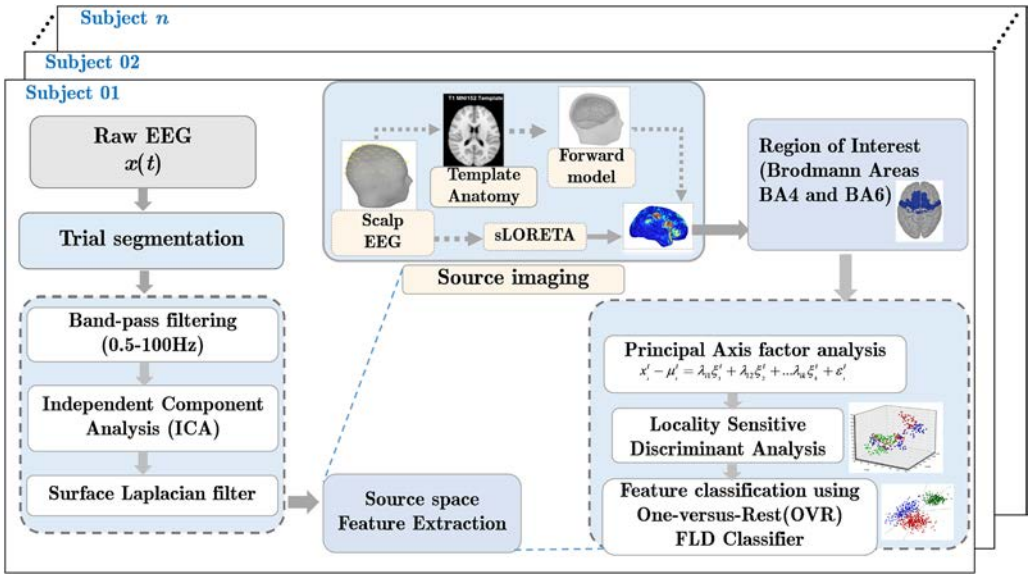

Figure 2. Procedural block diagram describing the proposed source-space feature extraction. Raw EEG data extracted from 118 electrodes are preprocessed as shown, followed by source-space feature extraction. An expanded view of source-space feature extraction (sub-block) is shown in the right half of the figure. The schematic shows inverse modeling using the sLORETA technique followed by the selection of anatomical ROIs in the Brodmann atlas (BA4, BA6). Forward modeling of EEG data is shown in the top pipeline of the source imaging block. It involves the EEG sensor montage and ICBM152 template anatomy and a three-layer realistic-geometry head model. Cortical time-series information is downsampled into designated ROIs (BA4 and BA6) for further feature extraction and classification.

into uniform epochs of 2 s each, with a baseline of 1 s (−1 to 0 s) and movement for 1 s (0–1 s), thus covering movement preparation and execution. It is to be noted that the subjects were instructed to finish their movement within 0.5 s, therefore the EEG corresponding to 0.5–1 s gives us the post-movement information. Raw EEG data from all 118 channels were band-pass filtered between 0.5 and 100 Hz using a 14th-order Chebyshev Type-2 filter. Artifact correction was done using independent component analysis (ICA) with the help of EEGLAB toolbox [37]. ICA was implemented using an extended infomax algorithm applied to all 118 EEG channels across 160 concatenated trials corresponding to four different classes, where each trial epoch was of duration 2 s. Artifact removal involves visual inspection of every independent component (IC), which is a tedious process. The ADJUST (automatic detector–joint use of spatial and temporal features) plug-in extension to the EEGLAB toolbox was used [38] to avoid the time-consuming process of manual inspection of all ICs. ADJUST is an automated artifact detection algorithm that uses various statistical measures such as spatial average difference (SAD) score, maximum epoch variance (MEV) and temporal kurtosis (TK) to identify eye-related artifacts such as eye blinks, horizontal and vertical eye movements, and other generic discontinuities. Independent components that were identified as artifacts by the ADJUST plugin were then removed, followed by interpolation of removed components. EOG artifacts were also removed by finding the artifact components that are highly correlated with the recorded EOG. The rest of the data were then back-projected into the sensor space. Subsequently, the local surface Laplacian filter was applied to the data as it is found to be robust in separating out muscle artifacts [39].

3. Methods

3.1. EEG source imaging

EEG source localization requires transforming the sensor domain into the source domain, even though the number of cortical sources vastly outnumber the number of scalp electrodes. This ill-posed problem has to be solved using several constraints and *a priori* information about the cortical region of interest. To convert EEG data from the sensor domain to the source domain we require a forward head model and a subsequent inverse solution. A simple analysis pipeline of our proposed method is illustrated in figure 2.

3.1.1. Forward modeling. Forward modeling is a critical stage in source imaging as it affects the accuracy of EEG source localization results substantially. The forward model is the subject's head model that can determine the scalp measurements, provided the locations of cortical sources are known. Various physical properties such as geometrical shape, conductivity values of different layers of the brain and also the number of voxels (3D volumetric pixels) are considered in the forward model. To achieve good source localization accuracy, we consider local anisotropies in different layers of the brain with the following conductivity values: 0.018 S m^{-1}, 0.44 S m^{-1} and 0.25 S m^{-1} for the skull, scalp and cortex, respectively [12]. A template anatomy of the International Consortium for Brain Mapping (ICBM-152) co-registered in MNI (Montreal Neurological Institute) space is used for the forward model [40]. After that, the template head model is warped to fit the template MNI anatomy of a subject using the Neuroscan template 3D digitized locations of all 118 channels used in the study. It is suggested that when a subject's MRI is not available, EEG source localization should include a multilayer

BEM with a realistic estimate of conductivity values and warped to co-registered electrode positions [41]. Previous studies have shown that the template anatomy can still provide comparable results in the case of group analysis [42, 43]. Following this, the cortical surface is tessellated into a triangular mesh composed of 15 002 vertices. A BEM is computed to achieve this tessellation using the OpenMEEG toolbox [44], which is reported to be reasonably accurate and also easier and faster to compute than the finite element method [45]. Solving this forward model results in a lead field matrix (Θ_f) that is essentially a subspace transformation matrix that transforms the sensor-space EEG into cortical source space. Mathematically, we can represent EEG source modeling as

$$\Omega = \Theta_f J + \varepsilon \tag{1}$$

where Ω is the sensor-space EEG recorded from N channels and Θ_f is the lead field matrix (LFM) of size $N \times m$ ($m \gg N$). Θ_f describes the propagation of current from source dipoles (m) to each scalp electrode (N). J is an $m \times t$ matrix of source dipole time series and ε is the noise perturbation matrix with covariance matrix Ψ. Task-independent signal information from the pre-stimulus baseline period (-1 to 0 s) is used to compute the noise covariance matrix.

3.1.2. Inverse modeling. We used a standardized low-resolution electromagnetic tomography (sLORETA)-based current density estimation technique using the BrainStorm Toolbox [46] for inverse modeling. sLORETA is a variant of the weighted minimum norm estimation technique for an inverse solution [10].

3.1.3. Region of interest. For a balanced run-time complexity and memory demand, we define a cortical ROI that contains source dipoles mostly correlated with a movement-related parameter like direction. For this purpose, a ROI is chosen from the anterior and posterior primary motor cortex (M1) spatially segregated in the Brodmann atlas, referred to as BA4a and BA4p, respectively. Also, the voxels belonging to Brodmann area 6 (BA6) that comprises premotor cortex (PMC) and a part of the supplementary motor area (SMA) are also selected as they are reported to be associated with movement involving spatial targets [47, 48]. From a warped cortical surface obtained after performing forward modeling, a total of 410 voxels corresponding to the ROI mentioned above are chosen for further analysis. It has been reported that the motor area specific to arm movement execution and imagery (also known as the hand knob region) is located near the precentral gyrus [14, 49].

3.2. Factor analysis-based EEG modeling

It is known that many cortical sources synchronize/desynchronize during certain tasks. A certain degree of correlation exists between cortical sources belonging to a region associated with similar functionality. However, each of these source dipoles is unique to some extent, thus resulting in a complex neural mechanism for every task. Therefore, we need a mathematical model that can describe this distinction between the commonality and the uniqueness of each source dipole. Factor analysis is one such method that is rarely investigated in the context of non-invasive EEG source-space analysis. Factor analysis is useful for extracting the behavioral information that is common across source dipoles of a similar ROI and also to get some insight into the unique behavior within the source dipoles of interest. Especially for the relatively challenging task of classifying different directions of arm movement, it is critical to understand which neuronal cluster contributes towards the movement in a particular direction. Hereafter, we describe the mathematical framework for understanding factor analysis as an unsupervised approach followed by our contribution that embeds a supervised approach for the same.

Consider an EEG trial i recorded from N sensors for t time samples. After inverse modeling, we have m source dipoles as random variables, $x_1, x_2, x_3, ..., x_P$, with respective means $\mu_1, \mu_2, \mu_3, ..., \mu_P$. A mathematical model of factor analysis is expressed as

$$x_i^t - \mu_i^t = \lambda_{i1}\xi_1^t + \lambda_{i2}\xi_2^t + ...\lambda_{ik}\xi_k^t + \varepsilon_i^t. \tag{2}$$

Here ξ denote common factors signifying the non-zero correlation between factors and λ_{ij} ($j = 1, 2, ..., k$) denotes factor loading. Note that there are certain assumptions that are natural consequences of the objectives of factor analysis. ε_i refers to the unique factor independently distributed with zero mean ($E(\varepsilon_i) = 0$) with a finite variance ψ, thus resulting in $\mathrm{Cov}(\varepsilon) = \mathrm{Diag}(\psi_1, \psi_2, \psi_3, ..., \psi_P)$. The diagonal covariance $\mathrm{Cov}(\varepsilon) = \Psi$ signifies the heteroscedastic noise that somewhat better explains the biological noise model as it does not make any assumption of identical noise variance for all sources. As the noise model is crucial in source imaging [50], it is desirable to select a model that can explain the data reasonably well. Both common factors and unique factors are important in factor analysis as they explain the shared behavior and the unique behavior of cortical sources. Unlike maximum likelihood estimation (MLE)-based factor extraction, we have chosen the principal axis method (PAM) as there is no need to assume a normal distribution in the noise model [51].

In matrix form, we can model the factor analysis as follows:

$$\bar{x} = \lambda\xi + \varepsilon \tag{3}$$

computing the covariance of both sides:

$$\begin{aligned} \Sigma &= \mathrm{cov}(\lambda\xi) + \mathrm{cov}(\varepsilon) \\ \Sigma &= \Lambda\,\mathrm{cov}(\xi)\Lambda' + \Psi \\ \Sigma &= \Lambda\mathrm{I}\Lambda' + \Psi \\ \Sigma &= \Lambda\Lambda' + \Psi. \end{aligned} \tag{4}$$

Since λ_{ij} is the (ij)th element of Λ, we can algebraically represent (4) as $\mathrm{cov}(\bar{x}_i, \xi_i) = \Lambda$, and it follows that the correlation of $\bar{x}_i$ and Ψ_i as $\mathrm{corr}(\bar{x}_i, \xi_i = \lambda_{ij})\ \forall\, i \in 1, 2, 3, ..., m, j \in 1, 2, 3, ..., p$ is

$$\begin{aligned} \sigma_{ii} &= \mathrm{var}(x_i) = (\lambda_{i1}^2 + \lambda_{i2}^2 + \lambda_{i3}^2 + ...\lambda_{im}^2) + \psi_i \\ &= h_i^2 + \psi_i. \end{aligned} \tag{5}$$

Further, (5) can be partitioned into two components: the first component representing the common factors (h_i^2), called 'communality', and the second unique to ψ_i, called

'specific variance'. Note that the covariance matrix Σ cannot be expressed exactly as shown in (4), i.e. Ψ as a diagonal matrix. Factor analysis involves the correlation matrix R modeled as an estimated Σ. Therefore, we use an estimator that will best approximate (4) as

$$R \cong \hat{\Lambda}\hat{\Lambda}' + \hat{\Psi}. \tag{6}$$

By applying singular value decomposition on $R - \hat{\Psi}$, we decompose Λ into CDC' (spectral decomposition) where the normalized eigenvectors of $R(c_i'c_i = 1)$ form an orthogonal matrix C and a diagonal matrix D with eigenvalues $\theta_1, \theta_2, \theta_3, ..., \theta_p$ as its diagonal entries.This matrix D can be decomposed into $D^{1/2}D^{1/2}$, and therefore the spectrally decomposed product CDC' (or $CD^{1/2}D^{1/2}C'$) can be factored in the form of $\hat{\Lambda}\hat{\Lambda}'$ as $(CD^{1/2})(CD^{1/2})'$. As Λ is of the form $p \times m$ $(m < p)$, only the top m eigenvalues of $D(\theta_1, \theta_2, \theta_3, ..., \theta_p)$, and their corresponding eigenvectors $C_1 = (c_1, c_2, c_3...c_m)$ are considered. Therefore, $\hat{\Lambda}$ can be written as $c_1\sqrt{\theta_1}, c_2\sqrt{\theta_2}, , \ldots, c_m\sqrt{\theta_m}$. Now, R can be represented as [52],

$$\hat{\Psi}_{ii} \cong R_{ii} - \sum_{j=1}^{m} \hat{\lambda}_{ij}^2. \tag{7}$$

Following the extraction of factors, they are sorted in a descending fashion indicating their relative contribution towards the variance in a given trial. This means that the subset of factors that explain most of the variance (90% for example) in a given trial will be considered for further analysis. Since these subsets of factors correspond to the source dipoles within the ROI, they preserve the neurophysiological relevance of the experimental task.

3.2.1. Supervised factor analysis for feature extraction. As the approach used so far is unsupervised, we plan to train a model to cluster a group of source dipoles $x_i(i = 1, 2, ..., j...P)$ as indexed by factors and class labels. We use the spatial information of a given dipole x_i in terms of its coordinates $S(x_i) = x_i(x, y, z)$ to compute the Euclidean distance. Thereafter, we use a class-wise label for every training trial t, as $l(t) = 1, 2, 3, 4)$ corresponding to the directional cues north, south, east and west, respectively. We define a within-class graph (G_w) and a between-class graph (G_b) to analyze the local neighborhood of nodes (source dipoles), where each node is assigned a weight as per the kernel function shown in (8) and (9) [53]:

$$W_{w,ij} = \begin{cases} (1 + \exp(-\dfrac{\|x_i - x_j\|^2}{\beta}) & \text{if } x_i \in N(x_j) \text{ and } l(x_i) = l(x_j) \\ 0 & \text{otherwise} \end{cases} \tag{8}$$

$$W_{b,ij} = \begin{cases} (1 - \exp(-\dfrac{\|x_i - x_j\|^2}{\beta}) & \text{if } x_i \in N(x_j) \text{ and } l(x_i) \neq l(x_j) \\ 0 & \text{otherwise} \end{cases} \tag{9}$$

where $W_{w,ij}$ denotes the weight of the within-class graph and $W_{b,ij}$ denotes the weight of the between-class graph. β is a Gaussian kernel parameter $(0 < \beta < 1)$ that controls the rate of decay. If x_i and x_j are neighboring dipoles and belong to the same class, then the within-class graph (G_w) will be assigned a non-zero weight. Similarly, a non-zero weight will be assigned to the neighboring nodes in the between-class graph (G_b) if those nodes belong to a different class.

We can represent the source space EEG as $y_i = A^T x_i + \epsilon$, where the optimization problem to solve for the maximization of inter-class and minimization of intra-class separation can be defined as:

$$\min \frac{1}{2} \sum_{ij} (y_i - y_j)^2 W_{w,ij} \tag{10}$$

$$\max \frac{1}{2} \sum_{ij} (y_i - y_j)^2 W_{b,ij} \tag{11}$$

$$\min \sum_{c=1}^{C} \sum_{j=1}^{n_c} (y_j^c - \mu_c)^2. \tag{12}$$

The combined objective function of (10)–(12) is shown in (13) [54] (for derivation, please refer to the appendix)

$$\begin{aligned} &\arg\max A^{\mathrm{T}} X(\alpha L_b + (1 - \alpha) W_w) X^{\mathrm{T}} A \\ &\text{s.t. } A^{\mathrm{T}} X D_w X^{\mathrm{T}} A = 1 \end{aligned} \tag{13}$$

where α is a shrinkage regularization parameter with an analytical solution [55]. The diagonal matrix corresponding to the column sums of W_w and W_b is denoted as D_w and D_b. L_b is the Laplacian matrix computed as $D_b - W_b$. Then we compute the transformation matrix A by applying the Lagrangian multiplier γ on (13) to solve the eigenvalue problem shown in (14) [56]:

$$A^{\mathrm{T}} X(\alpha L_b + (1 - \alpha) W_w) X^{\mathrm{T}} A = \gamma A^{\mathrm{T}} X D_w X^{\mathrm{T}} A. \tag{14}$$

Eigenvalue decomposition of A corresponding to the training set gives us the feature matrix. The proof of the solution to an eigenvalue problem shown in (14) is explained in the appendix. These features corresponding to the eigenvector $(a_1, a_2, ..., a_d)$ are used for classified using Fisher's linear discriminant classifier (FLD) [57].

3.3. Benchmarking algorithms

To compare our approach with existing methods, we examine different variants of a popular spatial filter algorithm called 'common spatial patterns' (CSP). Mathematically, the objective function of CSP $(J(w))$ has the form of a generalized Rayleigh quotient [2]. $J(w)$ tries to maximize the variance of one class and minimize the variance of another class as shown by the following [2]:

$$J(w) = \frac{w^T C_1 w}{w^T C_2 w} \tag{15}$$

where C_i denotes the covariance matrix of the ith class and w denotes the spatial filter.

One of the limitations of CSP is its sensitivity to over fitting; as a result, there is a need for regularization. One of the approaches is to use a Tikhonov-regularized CSP (TRCSP)

Table 1. Percentage classification accuracies for four-class classification resulting from different benchmarking algorithms.

	CSP (sensor)	TR-CSP (sensor)	SR-CSP (sensor)	CSP (source)	TR-CSP (source)	SR-CSP (source)	SFA (source)
S01	36.87	56.12	54.37	67.87	70.87	53.5	88.3
S02	34.12	30.87	49.25	36	48.25	63.12	73.67
S03	35.75	51.37	57.37	56	59.5	67.62	68.67
S04	29	34.75	47	30.87	63	67.25	72.37
S05	33	35.75	47	38.12	51.5	56.5	61.31
S06	38.37	51.12	44	49	67.12	59.87	78.06
S07	37.25	45.28	66.42	51.71	62.71	71.28	58.29
Mean	34.91	43.61	52.20	47.08	60.42	62.73	**71.52**

that adds a regularization term to an objective function $J(w)$ as shown in (16); another approach is to use shrinkage regularized CSP (SRCSP) that penalizes the covariance matrix (C_i) as shown in (17) [58]:

$$\hat{J}(w) = \frac{w^T C_1 w}{w^T C_2 w + \alpha P(w)} \tag{16}$$

$$C_c = (1-\gamma)C_i + \gamma I. \tag{17}$$

Here α is the regularization parameter for TRCSP and γ is the regularization parameter for SRCSP. Tikhonov regularization is often used to penalize a solution with large weights. It applies quadratic penalties $P(w)$ to regularize the objective function $J(w)$, and the results show that TRCSP is more efficient than CSP amongst other regularization approaches [58]. We chose the regularization parameter for TRCSP (α) empirically as 10×10^{-4} instead of cross-validation as it is computationally expensive. In contrast, SRCSP does not need cross-validation or heuristics for parameter selection (γ) as it has a closed-form analytical solution obtained using Ledoit and Wolf's method [59]. The SRCSP approach is reported to provide better results, especially when the training dataset is small [55].

Since the traditional CSP is well-suited for two-class problem, we used one-versus-rest (OVR) approach to extract multi-class features corresponding to four directions. So, the covariance matrix C_1 is calculated for trials corresponding to class i, while C_2 is calculated for all the trials belonging to the other classes, i.e. $j \neq i$. After solving the eigendecomposition problem for W, features $F_p(p = 1,...,2m)$ are calculated as

$$F_p = \log\left(\left[\mathrm{var}(Z_p)/\sum_{i=1}^{2m}\mathrm{var}(Z_p)\right]\right) \tag{18}$$

where E are time-series data and Z is the resultant subspace obtained by multiplying E with the spatial pattern matrix W. Only first and last two spatial filters ($m = 2$) of W are used for feature computation. Subsequently, these multi-class features are classified using the FLD classifier [57] with the OVR approach.

3.4. Statistical analysis

We assessed the classification performance of the proposed method using one-way repeated measures ANOVA. The type of feature space (sensor or source) is considered as a between-subjects factor (condition) with different regularization methods (CSP, TRCSP, SRCSP) as 'levels'. Further, one-way ANOVA corrected for multiple comparisons is also performed to observe the significance across feature extraction methods considering the decoding accuracy as a dependent variable. Post-hoc tests were done using a Tukey honestly significance difference (HSD) test. To establish the statistical significance of the proposed method, we set the significance level at $p < 0.05$. All statistical tests are performed using the SPSS software.

4. Results

4.1. Classification performance of source-space features

To assess the performance of our method in classifying different directions, we compared the cross-validation performance with other traditional sensor-space techniques. As mentioned in 3.3, we used the FLD classifier while not rejecting any of the trials. To ensure robustness, we performed cross-validation of the whole dataset by taking 80% of the trials as a training set and the remaining 20% as a test set; this was then repeated five times by randomizing the order of trials. We used this 5×5 cross-validation percentage accuracy as the criterion for evaluating different methods that are tabulated in table 1, and a box plot of the same is shown in figure 3.

Individual subject-wise decoding accuracy is shown as a small jitter next to each box plot. The legends in figure 3 show different feature extraction techniques. All the feature extraction methods used in this study could classify with a decoding accuracy higher than the chance level (25%) for four-class classification. One-way ANOVA of classification accuracies resulting from various feature extraction methods revealed $F(1,7) = 14.1541$ with a p-value of $9.7 \times 10e^{-9}$ suggesting that one or more treatments are significantly different. However, these results overestimate the significance, and therefore Tukey HSD tests for multiple comparisons were performed. Tukey HSD tests revealed that at least one or more pairs of treatments (feature extraction methods) are significantly different. Pairwise comparisons of our proposed method and the rest showed statistically significant results except for SRCSP in the source space ($F = 3.305$; $p > 0.05$). Furthermore, two-way repeated measures ANOVA with within-subject effects (sensor and source space), and three levels (CSP, TRCSP, and SRCSP) revealed a significant difference ($F = 54.683$;

Figure 3. Performance assessment of different feature extraction algorithms in terms of 5×5 cross-validation accuracy of classifying the EEG corresponding to hand movement in four directions. The *X*-axis indicates different feature extraction algorithms with feature space (sensor/source) highlighted in braces. The *Y*-axis indicates the average 5×5 cross-validation percentage accuracy. Jittered points indicate the decoding accuracy of individual subject.

$p < 0.001$) between the two effects. Tests of between-subject effects of three feature extraction methods with Bonferroni correction for multiple comparisons showed significant differences ($F = 8.654$, $p = 0.002$).

4.2. Source activation of hand movement in different directions

The results of sLORETA source localization showed cortical activation of movement of the right hand in different directions. A prior knowledge of anatomical ROI is an advantage as it can be used to validate our results. To illustrate this, we present the trial-averaged response of subject S01 from the source dipoles confined to Brodmann areas BA4aL, BA4pL and BA6L in figure 4. The stereotactic coordinates to plot this time series are shown in table 2. The most representative source dipole of these ROIs (BA4aL, BA4pL and BA6L) is shown as 3D stereotactic coordinates used in the forward model. Furthermore, to avoid the bias of prior neurophysiological information about the motor task to reflect the cortical functioning, we have shown the full brain activation on the cortex surface in figure 5.

4.3. Source dipoles corresponding to hand movement in different directions

In this section, we illustrate the use of a factor analytic approach to visualize the source dipoles influencing the task. Although there are 410 dipoles chosen from Brodmann areas BA4a, BA4p and BA6 from both hemispheres, very few dipoles would essentially result in significant variance. In this study we have considered a false discovery rate (FDR) of $p < 0.01$ as the criterion for selecting the dipoles based on the factor loading obtained from the supervised factor analysis. A FDR of $p < 0.01$ allows us to limit the number of false-positive source dipoles corresponding to a given directional cue. During different cross-validation runs for each subject, the number of dipoles selected after applying the statistical criterion is not constant. We observed that, on average, around 10 dipoles remained after the FDR-based criterion is applied. For the purpose of illustration, we have shown the dipoles corresponding to hand movement in different directions of one of the subjects (S01) in the form of colored nodes in figure 7 using BrainNet software [60].

4.4. Spectral–temporal characteristics of multidirectional movement decoding

EEG source activations exhibited direction-specific movement-related modulation. To illustrate this, we have plotted the time-series information of ROIs (Brodmann areas BA4aL, BA4pL, and BA6L) in figure 4. One can observe a clear peak in at least one of the Brodmann areas (BA4aL, BApL, and BA6L) at around 0.3–0.5 s after onset, which also shows that the anatomical ROIs have a temporal correlation with the actual movement duration of 0.5 s. To investigate the spectral characteristics of source imaging, we band-pass filtered the cortical time series in different frequency bands ranging from delta (<4 Hz) to high gamma (60–90 Hz). The spectral-domain responses are shown in figure 6 after computing the band power averaged over trials. In figure 6, each column indicates a different direction of movement and each row indicates a characteristic frequency band.

5. Discussion

5.1. Comparison of feature extraction techniques

In this study, we have introduced a supervised factor analytic approach to extract the cortical source space features for multi-direction hand movement classification. Extending the results obtained in sensor space, we found that the cortical source space features could be modeled so as to explain the variability as well as the similarity of source dipoles related to a given task. Regarding classification performance, our method outperforms traditional sensor-space spatial filter

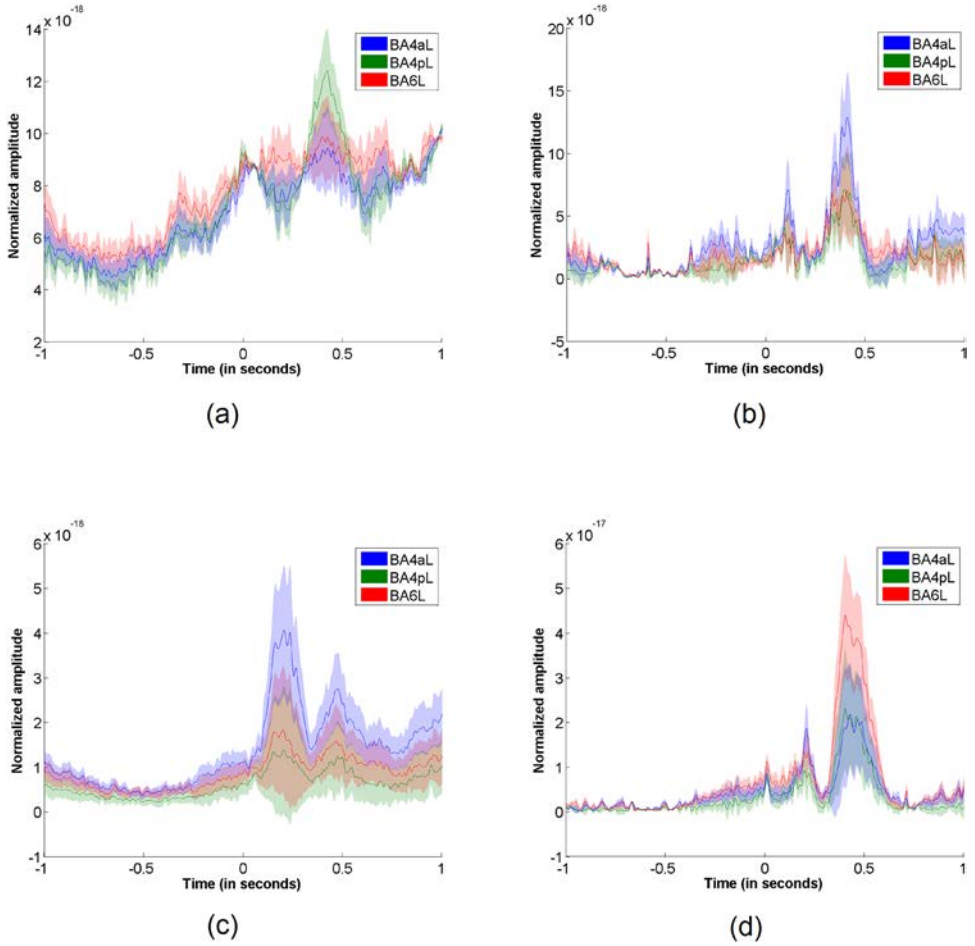

Figure 4. Trial-averaged response of subject S01 to four different directional cues in (a) east, (b) west, (c) north, and (d) south directions, respectively. Legends indicate stereotactic coordinates corresponding to the centroid of different Brodmann areas. These coordinates are further shown in table 1. Shading indicates the deviation from the mean response. The *X*-axis denotes the experimental timeline in seconds and the *Y*-axis the normalized amplitude resulting from sLORETA.

Table 2. Stereotactic coordinates of significant cortical activation.

		Coordinates		
Anatomical region of interest	Brodmann area nomenclature	*x*	*y*	*z*
Left anterior primary motor cortex (M1)	BA4a	80	107	138
Left posterior primary motor cortex (M1)	BA4p	62	117	123
Left preSMA	BA6	74	134	133

techniques such as regularized variants of CSP. We believe that the improvement in the classification accuracy compared with regularized variants of CSP could be because of the more discriminating spatial features in our proposed algorithm. The weights assigned to different source dipoles according to their relevance to the task label and neural anatomy add to the discriminability as compared with the spatial filters obtained from the traditional CSP approach. Our method is different from the CSP-based approach in the sense that CSP (and its regularized variants) maximizes the variance between two classes by solving the eigenvalue problem whereas our approach finds the most optimal eigenvalue corresponding to a given class (or task). As one can recall from (7), we extract the eigenvectors in a descending fashion corresponding to their relative contribution to the variance. In hindsight, CSP-based approaches derive the spatial filters based on the difference between the two classes as compared with task-specific neural correlates identified by our approach. Further, the weights assigned to each source node based on its neighborhood and the class label explain the task-specific feature extraction of our proposed method.

5.2. Contribution of the supervised factor analytic approach to source space feature extraction

In this study, we chose to use a factor analytic framework to construct a generative model that could reasonably describe how human cortical sources relate to the experimental task. Although we used a principal axis factor analysis-based approach to model the data that does not require a Gaussian

prior, there is a caveat that the factor analytic approach is iterative. Despite this caveat we have shown that our supervised factor analytic approach improves the classification performance quite significantly compared with the traditional feature extraction method. Our future approach would involve training an online adaptive classifier that learns the convergence parameters from previous sessions and subjects.

5.3. Cortical source activation of hand movement in different directions

Our present EEG source-space analysis indicates that the cortical activation related to hand movement in four orthogonal directions is spatially segregated within the motor area, primarily in the hand region of M1. Our findings concur with previous studies that report spatial segregation of populations of neurons that are directionally tuned [26, 27, 61]. Time-series information provided by brain scouts (BA4aL, BA4pL, and BA6L) in figure 4 reveal that the neuronal regions responsible for movement in different directions are indeed spatially segregated. It can be seen that the activation of the contralateral posterior primary motor cortex (BA4aL) is higher for movement in the 'east' direction, whereas contralateral anterior primary motor cortex (BA4pL) is more active during 'west' directional movement. Similarly, the contralateral pre-supplementary motor area (BA6L) is significant while moving the arm in the 'south' direction, in contrast to anterior primary motor cortex (BA4L) in the case of movement in the 'north' direction. Of course, this is not indicative of how every trial should look. It merely adds to our knowledge that spatial segregation of a relatively complex arm movement is indeed interpretable. Visualization of full-brain inverse modeling in figure 5 illustrates that the grand average results show significant activation in the cortical areas spanning the premotor cortex, primary motor cortex and superior frontal gyrus in the contralateral hemisphere of the brain. Even without any priors of specific anatomical regions, the observations are in line with the neurophysiological behavior of sensorimotor functions to validate our source imaging results.

5.4. Spectral characteristics of cortical activation corresponding to different directions

Spectral characteristics of movement-related tasks are always a subject of debate. Many researchers have shown the variations in the event related desynchronization/synchronization (ERD/S) spanning a wide range of frequencies. Although it is well-documented in the literature that the mu-rhythms are the frequencies of interest, there are also studies that report beta-band activity to be more consistent than the mu-band [62]. Although the experimental paradigms are not the same, it is still possible that beta and gamma rhythms might play an important role in multidirectional movement tasks. Therefore, we performed group analysis ($n = 7$) of broad-spectrum cortical activation (normalized amplitude of sLORETA) to investigate the spectral characteristics of source activation in terms of different characteristic frequency bands of EEG. Similar to the analysis done in section 4, we used full brain sLORETA

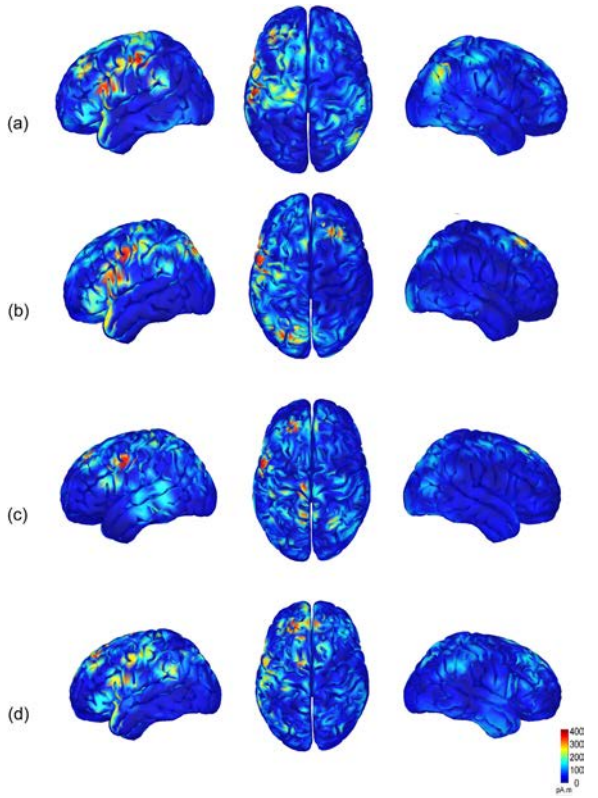

Figure 5. Group average cortical source maps of all subjects ($n = 7$, right handed). sLORETA source activation patterns resulting from hand movements in different directions (a) east, (b) west, (c) north, and (d) south. Cortical activation is shown in three orientations (from left to right): left lateral, dorsal and right lateral view of the cortex.

maps to analyze spectral characteristics. In figure 6, we show the contralateral view of grand average cortical activation across subjects in different frequency bands ranging from delta (0.5–4 Hz) to high gamma (60–90 Hz). From figure 6, it is evident that motor areas show higher activation in the delta, alpha and beta frequency ranges.

5.5. Contribution of source dipoles for a given task

From figure 7 we can observe that the spherical nodes are of different sizes that indicate their relative contribution to the variance. In simpler terms: the bigger the source node, the more significant its contribution to a given task. The significant source nodes are located along the precentral gyrus, although the anatomical region covers a much larger cortical surface. This visual illustration is subject specific, and the location of significant source nodes varies across subjects, albeit they all conform to the same anatomical ROI. Another interesting observation is that the significant nodes corresponding to the movement in 'north' and 'south' directions are relatively more concentrated towards the central region. From a neurophysiological perspective, there are more muscles and joints involved in moving one's arm in the 'north' and 'south' directions, which signifies neural activation corresponding to the elbow and shoulder. According to the concept of the motor homunculus, the elbow and shoulder have

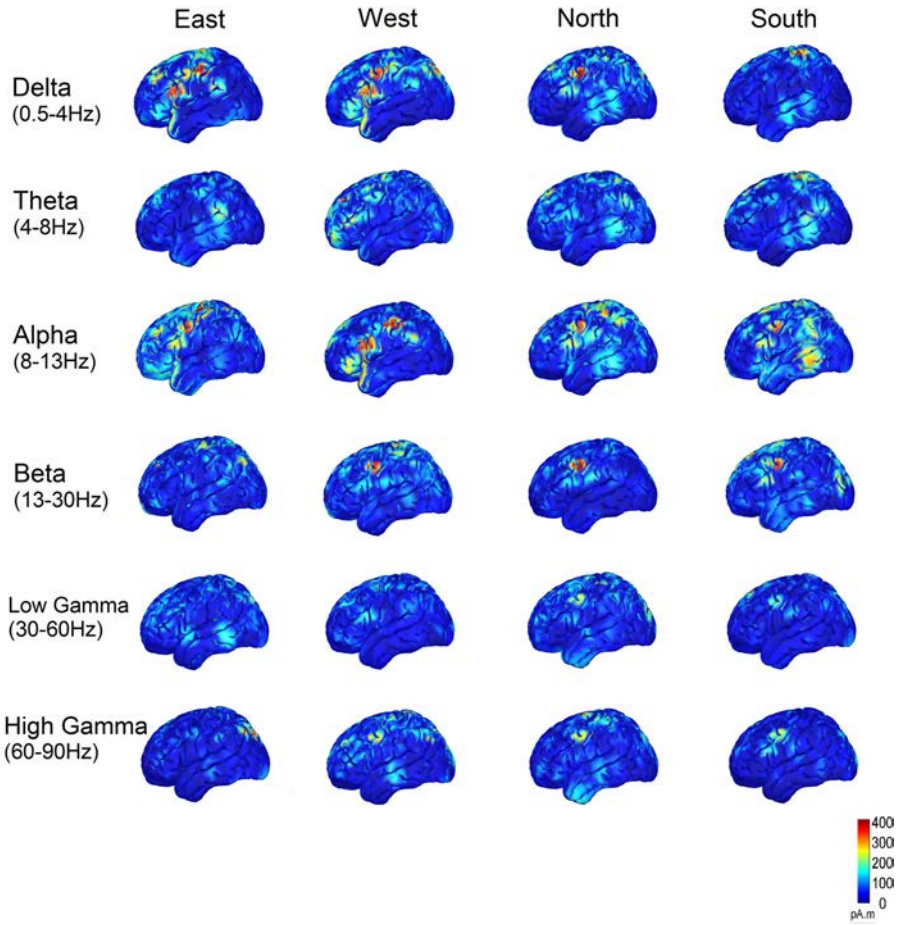

Figure 6. Left lateral view of group average sLORETA-based source activation maps corresponding to different frequency bands ranging from delta (0.5–4 Hz) to high gamma (60–90 Hz).

distinct neuronal activation regions in the central part of the brain, although they occupy a relatively smaller overlapping area of the cortex. Further, it would be interesting to go beyond the neural correlates and observe the causal interpretation of stimulus (direction cue) on the cortical activation in different frequency bands (aka effects).

5.6. Limitations

In our current study, we have used the subject-independent template anatomy that is available from the MNI website, as we did not have subject-specific MRIs. Although there are studies which have reported robust forward modeling results from the template anatomy, it would be worth investigating the effect of the data-driven forward model proposed in [63]. Furthermore, our study involved predefined ROIs based on well-documented literature concerning motor tasks. Note that the process is not completely automatic as it still requires manual intervention. Although manual ROI selection tends to give a better justification of source-space results and also saves computation time due to the reduced feature dimension, it is not robust when a given experimental paradigm does not have a specific ROI concerned with the task. ROI-based feature extraction would not be very helpful for studies involving functional interference across neural

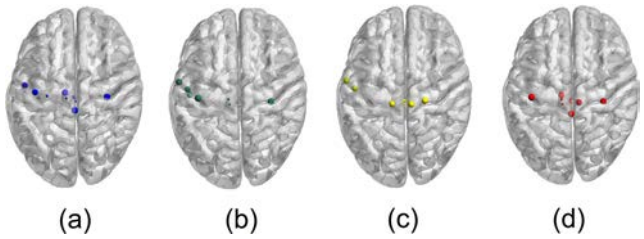

Figure 7. Subject-specific source dipoles selected using our proposed factor analytic method. FDR-corrected ($p < 0.01$) sources are shown in the form of spherical nodes corresponding to different directions: (a) east, (b) west, (c) north, and (d) south. Different sizes of these spherical nodes suggest their relative proportion of variance in factor loading.

regions during a complex cognitive task. Figure 5 illustrates that the full-brain cortical map point towards the active regions nearly overlapping the predefined cortical ROI, which implies that source localization is not sensitive to predefined regions. Further, it would be interesting to see how the features from data-driven ROI selection would affect the performance of our method. Our approach involved novel supervised learning for factor analysis that did not take into account any regularization of weights. There is a scope to regularize the objective functions, and this could lead to higher classification accuracies.

6. Conclusion

We have proposed a novel feature extraction method based on supervised factor analysis that considers the somatotropic organization of hand movement in four orthogonal directions. A mathematical framework based on supervised factor analysis is used to classify movement in four directions. In scenarios where decoding the motor actions with higher degrees of freedom is of paramount importance, prior knowledge of neurophysiology can aid in translating brain signals into control commands for effectors. Although it is difficult for current state-of-the-art brain-controlled devices to perfectly mimic real human arm functionalities, the development of more robust movement-decoding algorithms in the future will certainly push the boundaries of traditional neurorehabilitation practices based on BCI. The present work on multi-directional arm movement classification using cortical EEG features is a contribution in this direction. Compared with conventional methods that use sensor-space features, our source-space features resulted in an improvement of more than 10% in the classification accuracy. Previous work from our group [22] emphasized improving the classification accuracy of four-directional movement classification by using different regularized approaches in wavelet-common spatial patterns in the EEG sensor space. In contrast, our current method emphasizes the cortical source distribution inferred from sLORETA inverse modeling. As a result, our method provides more information about the neurophysiological aspects of right hand movement in four orthogonal directions. Further, we present the formulation of supervised factor analysis that takes spatial information of source dipoles into account to preserve the local information of anatomical ROIs. The confinement of the ROI to motor regions helps not only to reduce the computation time significantly but also to achieve substantially higher classification accuracy than that of the sensor-space features. Different statistical tests revealed that source-space features enhance the classification accuracy of multidirectional hand movement.

Our future work will emphasize further improvement in classification accuracy by embedding the regularized approaches to factor analytic methods. For a better interpretation of more complex tasks, we plan to use causal inference algorithms [64] to model the factor analytic problem in (2). Another interesting direction is online BCI for stroke rehabilitation, where real-time cortical imaging can be used to get more information about cortical activation over a period. We look forward to employing adaptation algorithms to learn across experimental sessions to reduce the overall computation time. With the advent of real-time source localization algorithms we are hopeful that our work will pave a new direction in interpreting the results of EEG-based BCI.

Appendix

In this appendix, we derive the expression for the eigenvalue problem in (13) by optimizing the objective functions (10)–(12),

$$\begin{aligned}
&\min \frac{1}{2}\sum_{ij}(y_i - y_j)^2 W_{w,ij} \\
&= \min \frac{1}{2}\sum_{ij}((A^{\mathrm{T}}x_i + \varepsilon) - (A^{\mathrm{T}}x_j + \varepsilon))^2 W_{w,ij} \\
&= \min \sum_{i} A^{\mathrm{T}}x_i D_{w,ii} x_i^{\mathrm{T}} A - \min \sum_{ij} A^{\mathrm{T}}x_i W_{w,ij} x_j^{\mathrm{T}} A \\
&= \min A^{\mathrm{T}} X(D_w - W_w) X^{\mathrm{T}} A \\
&= \min A^{\mathrm{T}} X L_W X^{\mathrm{T}} A
\end{aligned} \tag{A.1}$$

$$\begin{aligned}
&\max \frac{1}{2}\sum_{ij}(y_i - y_j)^2 W_{b,ij} \\
&= \max \frac{1}{2}\sum_{ij}((A^{T}x_i + \varepsilon) - (A^{T}x_j + \varepsilon))^2 W_{b,ij} \\
&= \max \sum_{i} A^{T}x_i D_{b,ii} x_i^{T} A - \max \sum_{ij} A^{T}x_i W_{b,ij} x_j^{T} A \\
&= \max A^{T} X(D_b - W_b) X^{T} A \\
&= \min A^{T} X L_b X^{T} A.
\end{aligned} \tag{A.2}$$

From (12), we have

$$\begin{aligned}
&\min \sum_{c=1}^{C}\sum_{j=1}^{n_c}(y_j^c - \mu_c)^2 \\
&= \min \sum_{c=1}^{C}(\sum_{j=1}^{n_c}(y_j^c - \mu_c)(y_j^c - \mu_c)^{\mathrm{T}}) \\
&= \min \sum_{c=1}^{C}(\sum_{j=1}^{n_c}(y_j^c y_j^{c\mathrm{T}} - \mu_c y_j^{c\mathrm{T}} - y_j^{c\mathrm{T}}\mu_c + \mu_c \mu_c^{\mathrm{T}})) \\
&= \min \sum_{c=1}^{C}(\sum_{j=1}^{n_c}(y_j^c y_j^{c\mathrm{T}} - n_c \mu_c \mu_c^{\mathrm{T}})) \\
&= \min \sum_{c=1}^{C}(\sum_{j=1}^{n_c}(y_j^c y_j^{c\mathrm{T}} - \frac{1}{n_c}(y_1^c + ...y_{n_c}^c)(y_1^c + ...y_{n_c}^c)^{\mathrm{T}})) \\
&= \min \sum_{c=1}^{C}(\sum_{j=1}^{n_c}(Ax_j^c)(Ax_j^c)^{\mathrm{T}} - \frac{1}{n_c}(A^T x_1^c + ...A^T x_{n_c}^c)(A^T x_1^c + ...A^T x_{n_c}^c)^T) \\
&= \min A^T \sum_{c=1}^{C}(X_c(I - \frac{1}{n_c}e_c e_c^T)X_c^T A.
\end{aligned} \tag{A.3}$$

The combined optimization problem of (A.1)–(A.3) can be defined as:

$$\begin{aligned}
&\arg\max A^{\mathrm{T}}(P - \alpha S_w)A \\
&\text{s.t.}\, A^{\mathrm{T}}A = I
\end{aligned} \tag{A.4}$$

where $P = X(L_b - L_w)X^T$, $S_w = \sum_{c=1}^{C} X_c\left(I - \frac{1}{n_c}e_c e_c^T\right)X_c^T$ and e_c is a n-dimensional identity vector. A Lagrangian multiplier is applied on the objective function (A.4) to obtain the optimal transformation matrix A as:

$$\frac{\partial}{\partial A}(A^{\mathrm{T}}(P - \alpha S_w)A - \lambda(A^{\mathrm{T}}A - I)) = 0. \tag{A.5}$$

Further, (A.4) is converted into an eigenvalue problem as

$$(P - \alpha S_w)A = \lambda A. \tag{A.6}$$

The eigenvalue problem in (A.6) is solved for the eigenvectors that are sorted in a descending order to give us the features for further classification.

References

[1] Van Den Broek S P, Reinders F, Donderwinkel M and Peters M J 1998 Volume conduction effects in EEG and MEG *Electroencephalogr. Clin. Neurophysiol.* **106** 522–34

[2] Blankertz B, Losch F, Krauledat M, Dornhege G, Curio G and Müller K-R 2008 The Berlin brain–computer interface: accurate performance from first-session in BCI-naïve subjects *IEEE Trans. Biomed. Eng.* **55** 2452–62

[3] Handiru V S, Vinod A P and Guan C 2016 Multi-direction hand movement classification using EEG-based source space analysis *38th Annual Int. Conf. of the IEEE Engineering in Medicine and Biology Society* (IEEE) pp 4551–4

[4] Shenoy H V, Vinod A P and Guan C 2015 Cortical source localization for analysing single-trial motor imagery EEG *IEEE Int. Conf. on Systems, Man and Cybernetics* (IEEE) pp 3146–51

[5] He B, Yang L, Wilke C and Yuan H 2011 Electrophysiological imaging of brain activity and connectivity challenges and opportunities *IEEE Trans. Biomed. Eng.* **58** 1918–31

[6] Michel C M and Murray M M 2012 Towards the utilization of EEG as a brain imaging tool *NeuroImage* **61** 371–85

[7] Cuffin B N, Schomer D L, Ives J R and Blume H 2001 Experimental tests of EEG source localization accuracy in spherical head models *Clin. Neurophysiol.* **112** 46–51

[8] Ding L and He B 2006 Spatio-temporal EEG source localization using a three-dimensional subspace FINE approach in a realistic geometry inhomogeneous head model *IEEE Trans. Biomed. Eng.* **53** 1732–9

[9] Grech R, Cassar T, Muscat J, Camilleri K P, Fabri S G, Zervakis M, Xanthopoulos P, Sakkalis V and Vanrumste B 2008 Review on solving the inverse problem in EEG source analysis *J. Neuroeng. Rehabil.* **5** 25

[10] Pascual-Marqui R D 2002 Standardized low resolution brain electromagnetic tomography *Methods Findings Exp. Clin. Pharmacol. 24 Suppl.* **2002** 5–12

[11] Shirvany Y, Mahmood Q, Edelvik F, Jakobsson S, Hedstrom A and Persson M 2014 Particle swarm optimization applied to EEG source localization of somatosensory evoked potentials *IEEE Trans. Neural Syst. Rehabil. Eng.* **22** 11–20

[12] Song J, Davey C, Poulsen C, Luu P, Turovets S, Anderson E, Li K and Tucker D 2015 EEG source localization: sensor density and head surface coverage *J. Neurosci. Methods* **256** 9–21

[13] Yao J and Dewald J P A 2005 Evaluation of different cortical source localization methods using simulated and experimental EEG data *NeuroImage* **25** 369–82

[14] Edelman B J, Baxter B and He B 2016 EEG source imaging enhances the decoding of complex right-hand motor imagery tasks *IEEE Trans. Biomed. Eng.* **63** 4–14

[15] Ofner P and Müller-Putz G R 2015 Using a noninvasive decoding method to classify rhythmic movement imaginations of the arm in two planes *IEEE Trans. Biomed. Eng.* **62** 972–81

[16] Gu Y, Dremstrup K and Farina D 2009 Single-trial discrimination of type and speed of wrist movements from EEG recordings *Clin. Neurophysiol.* **120** 1596–600

[17] Liao K, Xiao R, Gonzalez J, Ding L and Zhang Z 2014 Decoding individual finger movements from one hand using human EEG signals *PLoS One* **9** e85192

[18] Yong X, Menon C, Wessel B, Hallet M, Cohen L and He B 2015 EEG classification of different imaginary movements within the same limb *PLoS one* **10** e0121896

[19] Xiao R and Ding L 2015 EEG resolutions in detecting and decoding finger movements from spectral analysis *Frontiers Neurosci.* **9** 308

[20] Hammer J, Pistohl T, Fischer J, Kršek P, Tomášek M, Marusič P, Schulze-Bonhage A, Aertsen A and Ball T 2016 Predominance of movement speed over direction in neuronal population signals of motor cortex: intracranial EEG data and a simple explanatory model *Cerebral Cortex* **26** 2863–81

[21] Robinson N, Vinod A P, Ang K K, Tee K P and Guan C T 2013 EEG-based classification of fast and slow hand movements using Wavelet-CSP algorithm *IEEE Trans. Biomed. Eng.* **60** 2123–32

[22] Robinson N, Guan C, Vinod A P, Ang K K and Tee K P 2013 Multi-class EEG classification of voluntary hand movement directions *J. Neural Eng.* **10** 01–11

[23] Yuan H, Perdoni C and He B 2010 Relationship between speed and EEG activity during imagined and executed hand movements *J. Neural Eng.* **7** 26001

[24] Zaepffel M, Trachel R, Kilavik B E and Brochier T 2013 Modulations of EEG beta power during planning and execution of grasping movements *PLoS One* **8** e60060

[25] Robinson N and Vinod A P 2016 Noninvasive brain–computer interface: decoding arm movement kinematics and motor control *IEEE Syst. Man Cybern. Mag.* **2** 4–16

[26] Cowper-Smith C D, Lau E Y, Helmick C A, Eskes G A and Westwood D A 2010 Neural coding of movement direction in the healthy human brain *PLoS One* **5** e13330

[27] Eisenberg M, Shmuelof L, Vaadia E and Zohary E 2010 Functional organization of human motor cortex: directional selectivity for movement *J. Neurosci.* **30** 8897–905

[28] Grosse-Wentrup M, Liefhold C, Gramann K and Buss M 2009 Beamforming in noninvasive brain–computer interfaces *IEEE Trans. Biomed. Eng.* **56** 1209–19

[29] Santhanam G, Yu B M, Gilja V, Ryu S, Afshar A, Sahani M and Shenoy K V 2009 Factor-analysis methods for higher-performance neural prostheses *J. Neurophysiol.* **102** 1315–30

[30] Harman H H 1976 *Modern Factor Analysis* (Chicago: University of Chicago Press)

[31] Schott G D 1993 Penfield's homunculus: a note on cerebral cartography *J. Neurol. Neurosurg. Psychiatry* **56** 329–33

[32] Bradberry T J, Gentili R J and Contreras-Vidal J L 2010 Reconstructing three-dimensional hand movements from noninvasive electroencephalographic signals *J. Neurosci.* **30** 3432–7

[33] Chestek C A, Gilja V, Blabe C H, Foster B L, Shenoy K V, Parvizi J and Henderson J M 2013 Hand posture classification using electrocorticography signals in the gamma band over human sensorimotor brain areas *J. Neural Eng.* **10** 026002

[34] Waldert S, Preissl H, Demandt E, Braun C, Birbaumer N, Aertsen A and Mehring C 2008 Hand movement direction decoded from MEG and EEG *J. Neurosci.* **28** 1000–8

[35] Seeber M, Scherer R, Wagner J, Solis-Escalante T and Müller-Putz G R 2015 High and low gamma EEG oscillations in central sensorimotor areas are conversely modulated during the human gait cycle *NeuroImage* **112** 318–26

[36] Krebs H I, Hogan N, Aisen M L and Volpe B T 1998 Robot-aided neurorehabilitation *IEEE Trans. Rehabil. Eng.* **6** 75–87

[37] Delorme A and Makeig S 2004 EEGLAB: an open source toolbox for analysis of single-trial EEG dynamics including independent component analysis *J. Neurosci. Methods* **134** 9–21

[38] Mognon A, Jovicich J, Bruzzone L and Buiatti M 2010 ADJUST: an automatic EEG artifact detector based on the joint use of spatial and temporal features *Psychophysiology* **48** 229–40

[39] Fitzgibbon S P, Lewis T W, Powers D M W, Whitham E W, Willoughby J O and Pope K J 2013 Surface Laplacian

of central scalp electrical signals is insensitive to muscle contamination *IEEE Trans. Biomed. Eng.* **60** 4–9
[40] Collins D L, Neelin P, Peters T M and Evans A C 1994 Automatic 3D intersubject registration of MR volumetric data in standardized Talairach space *J. Comput. Assist. Tomogr.* **18** 192–205
[41] Acar Z A and Makeig S 2013 Effects of forward model errors on EEG source localization *Brain Topogr.* **26** 378–96
[42] Eytan D, Pang E W, Doesburg S M, Nenadovic V, Gavrilovic B, Laussen P and Guerguerian A-M 2016 Bedside functional brain imaging in critically-ill children using high-density EEG source modeling and multi-modal sensory stimulation *NeuroImage* **12** 198–211
[43] Steinstraeter O, Teismann I K, Wollbrink A, Suntrup S, Stoeckigt K, Dziewas R and Pantev C 2009 Local sphere-based co-registration for SAM group analysis in subjects without individual MRI *Exp. Brain Res.* **193** 387–96
[44] Gramfort A, Papadopoulo T, Olivi E and Clerc M 2010 OpenMEEG: opensource software for quasistatic bioelectromagnetics *Biomed. Eng. Online* **9** 45
[45] Lei X, Wu T and Valdes-Sosa P A 2015 Incorporating priors for EEG source imaging and connectivity analysis *Frontiers Neurosci.* **9** 284
[46] Tadel F, Baillet S, Mosher J C, Pantazis D and Leahy R M 2011 Brainstorm: a user-friendly application for MEG/EEG analysis *Comput. Intell. Neurosci.* **2011** 879716
[47] Caminiti R, Johnson P B, Galli C, Ferraina S and Burnod Y 1991 Making arm movements within different parts of space: the premotor and motor cortical representation of a coordinate system for reaching to visual targets *J. Neurosci.* **11** 1182–97
[48] Kermadi I and Boussaoud D 1995 Role of the primate striatum in attention and sensorimotor processes: comparison with premotor cortex *Neuroreport* **6** 1177–81
[49] Szameitat A J, Shen S and Sterr A 2007 Motor imagery of complex everyday movements. An fMRI study *NeuroImage* **34** 702–13
[50] Engemann D A and Gramfort A 2015 Automated model selection in covariance estimation and spatial whitening of MEG and EEG signals *NeuroImage* **108** 328–42
[51] Rencher A C 2003 *Methods of Multivariate Analysis* (New York: Wiley) (https://doi.org/10.1111/insr.12020_20)
[52] Mulaik S A 2009 *Foundations of Factor Analysis* (Boca Raton, FL: CRC Press)
[53] Handiru V S, Vinod A P and Guan C 2016 A novel supervised locality sensitive factor analysis to classify voluntary hand movement in multi direction using EEG source space *IEEE Int. Conf. on Systems, Man, and Cybernetics* (IEEE) pp 2795–800
[54] Yi Y, Zhang B, Kong J and Wang J 2013 An improved locality sensitive discriminant analysis approach for feature extraction *Multimedia Tools Appl.* **74** 85–104
[55] Shenoy H V, Vinod A P and Guan C 2015 Shrinkage estimator based regularization for EEG motor imagery classification *10th Int. Conf. on Information, Communications and Signal Processing* (IEEE) pp 1–5
[56] Cai D, He X, Zhou K, Han J and Bao H 2007 Locality sensitive discriminant analysis *Proc. of the 20th Int. Joint Conf. on Artificial intelligence (Morgan Kaufmann Publishers Inc.) pp* 708–13
[57] Duda R O, Hart P E and Stork D G 2000 *Pattern Classification* (New York: Wiley) ISBN: 978-0-471-05669-0
[58] Lotte F and Guan C 2011 Regularizing common spatial patterns to improve BCI designs: unified theory and new algorithms *IEEE Trans. Biomed. Eng.* **58** 355–62
[59] Ledoit O and Wolf M 2004 A well-conditioned estimator for large-dimensional covariance matrices *J. Multivariate Anal.* **88** 365–411
[60] Xia M, Wang J and He Y 2013 BrainNet viewer: a network visualization tool for human brain connectomics *PLoS One* **8** e68910
[61] Toxopeus C M, de Jong B M, Valsan G, Conway B A, Leenders K L and Maurits N M 2011 Direction of movement is encoded in the human primary motor cortex *PLoS One* **6** e27838
[62] Seeber M, Scherer R, Wagner J, Solis-Escalante T and Muller-Putz G R 2014 EEG beta suppression and low gamma modulation are different elements of human upright walking *Frontiers Human Neurosci.* **8** 1–9
[63] Hansen S T, Hauberg S and Hansen L K 2016 Data-driven forward model inference for EEG brain imaging *NeuroImage* **139** 249–58
[64] Grosse-Wentrup M, Schölkopf B and Hill J 2011 Causal influence of gamma oscillations on the sensorimotor rhythm *NeuroImage* **56** 837–42